ORIGINAL ARTICLE



Interactions between subpolar and subtropical jet streams lead to extreme rainfall events over the North Indian Subcontinent in June 2013 and July 2023

Dipanjan Dey^{1,2} • Ligin Joseph² • Arkaprava Ray¹ • Robert Marsh² • Nikolaos Skliris² • Andrew G. Turner^{3,4} • D. C. Ayantika⁵ • Parthasarathi Mukhopadhyay⁶ • Arun Chakraborty⁷ • Sourav Sil¹

Received: 22 January 2025 / Accepted: 24 April 2025 / Published online: 13 May 2025 © The Author(s) 2025

Abstract

North Indian Subcontinent (NIS) is prone to disastrous and life-threatening floods during the summer monsoon period primarily due to its close proximity with the Himalayan foothills. Indian Meteorological Department (IMD) reported that during June 13-19, 2013, the Uttarakhand state in North India experienced a cumulative total of 322 mm rainfall, a 847% weekly departure against the long-term average rainfall (1971–2020) of 34 mm. After a decade, another state in the same region, Himachal Pradesh, received an unprecedented 223 mm of rainfall in just 4 days, viz 7-11 July 2023, a 436% deviation from the cumulative climatological rainfall of 41.6 mm for 4 days (July 7–11). It is shown that the atmospheric water vapor is transported towards NIS by two monsoon low pressure systems during the June 2013 event. In contrast, during the July 2023 flood, the monsoon trough shifted southward, resulting in the moisture transport pathway predominantly over the northern Indian Ocean. In conjunction, it was shown through upper-level air tracing that southward movement of the subpolar jet stream creates a trough in the subtropical jet stream, which intrudes along the western boundary of NIS, leading to upper-level divergence. This pattern was observed in both flood events. By leveraging the mass-conserving nature and unique capability of a Lagrangian tracing model to track atmospheric water backward in time, our novel analysis of the 2023 flood reveals that two evaporative sources near Madagascar and the western Indian Ocean were key contributors, and inland evaporation played a comparatively lesser role as compared to the 2013 case. The Bay of Bengal served primarily as a vapor transport pathway rather than a direct moisture source for both events. This novel Lagrangian approach, which exposes separate drivers of extreme monsoon rainfall, upstream and at lead times of days-weeks, has the potential to be used more extensively and operationally.

Keywords Indian monsoon · Extreme rainfall · Subpolar jet stream · Lagrangian tracing

1 Introduction

The seasonal reversal of wind patterns across South Asia forms two distinct monsoon systems in the region. In particular, on the Indian subcontinent, the southwest monsoon (June–September), often referred to as the Indian summer monsoon (ISM), has greater significance compared to the northeast monsoon due to its large spatial extent and economic impact. Crop yields in an agrarian country like India depend immensely on the spatio-temporal distribution of summer rainfall, which is majorly driven by various semi-permanent systems (e.g., monsoon trough, heat low, Tibetan

anticyclone, tropical easterly jet etc.), results in either of normal, deficit, or excess monsoon (Jenamani and Dash 2005). However, the occurrence of unusual extreme conditions during the ISM not only hinders economic progress but also causes massive loss of life and property. Such extreme conditions include both flooding and drought, where the flooding can be associated with riverine flood and flash flood due to excess monsoonal rainfall. A study based on the India Meteorological Department (IMD) data from 1978–2006, claimed the occurrence of a total of 2443 flood events, which caused a death toll of around 45,000 along with a damage of \$16 billion (Singh and Kumar 2013). Notably, 80% of these floods occurred during the summer monsoon season, accounting for 90% of total flood-related fatalities. Recent estimates from The Emergency Events Database (EM-DAT,

Extended author information available on the last page of the article



http://www.emdat.be) for the period 2000–2023 identified approximately 193 events over India impacting 360 million lives and causing damage worth of \$172 million.

The Himalayan region of India often encounters intense episodic rainfall events during the ISM (Joshi and Kumar 2006; Nandargi and Dhar 2012; Rana et al. 2013). However, whether that rainfall will translate into flooding depends on the geographical location. Most of the floods in north-east India, especially over Assam in recent times, are caused due to the presence of low-lying basins, vulnerable to overflow of both the Subansiri and Brahmaputra rivers (Gogoi et al. 2013). In contrast, the floods over the NIS Himalayan region are usually caused by the combined effects of atmospheric, cryospheric and geologic processes (Dimri et al. 2016). A composite study of 34 extreme rainfall events in the western Himalaya during only summer monsoon of 1979-2013, reveals the crucial role of extratropical and tropical monsoon circulation interaction (Vellore et al. 2016). Such interaction can be explained by a few key elements like the Rossby wave breaking (Hunt et al. 2018a; Vellore et al. 2020), north-northwest movement of monsoon synoptic systems and its interaction with western disturbances (Hunt et al. 2021), split pattern of Tibetan anticyclone (Vellore et al. 2020), and the strong convective elements over the foothills of Himalayas. A high-resolution modelling study indicated that the convergence of mid-latitude westerly winds and weak monsoon circulation during the monsoon break phase can cause high mid-tropospheric vorticity and precipitation over Himalayan foothills (Vellore et al. 2014). Another concurrent research also reported the existence of positive correlation between precipitation extremes and cyclonic disturbances, especially those formed over Bay of Bengal (BoB)(Revadekar et al. 2016). A recent study on cloudburst events (100 mm of rain in 1 h) using satellite data reveals that the Rossby wave pattern was different for each cloudburst events over the Himalayan regions of North India during 1981-2015 (Gupta et al. 2023). In addition to these composite analyses, few individual case studies were also performed to identify the atmospheric factors responsible for devastating floods over North India.

According to the IMD monsoon report of 2013 (Ray et al. 2014), one such catastrophic flood occurred between June 15th and 18th over Uttarakhand. The Indian state of Uttarakhand received a total rainfall of 322 mm from June 13th to 19th, which was 847% higher than its average value. This catastrophic event impacted around 100,000 local residents and claimed a loss of over 500 human lives (Ray et al. 2014; Kaur and Gupta 2017). According to reports from the Government of India, the Uttarakhand flood led to the loss of approximately 9,200 cattle/livestock and hundreds of animal shelters (https://india.mongabay.com/2018/06/fiveyears-since-uttarakhand-floods-continued-disregard-for-the-environment-is-an-open-invitation-for-more-calamities/). An

ecological damage assessment study by Rawat et al. (2016) revealed a substantial loss of 33.16 hectares of dense mixed forest and 59.28 hectares of open mixed forest in the Uttarakhand district due to torrential rainfall in June 2013. A detailed analysis using different observational and reanalysis dataset revealed that the displaced westerlies towards subtropics and the Rossby wave in mid-latitudes increased the wind speed ahead of the trough, resulting in divergence in the upper levels (200hPa). Consequently, strong anomalous low-level convergence formed over the region and together with the monsoon low pressure systems it maintained a constant flow of moisture from Arabian Sea and Bay of Bengal (Ranalkar et al. 2016). A previous study by Joseph et al. (2015) also referred to similar dynamics, responsible for the event, however their analysis further added the skill of Ensemble Prediction System (EPS) on predicting the event. They concluded that the EPS was able to detect the extreme event 10-12 days in advance but failed to capture the midlatitude influence and hence the correct rainfall amount. In addition to these outcomes, earlier studies also suggested the dominance of orographic lifting, which distinguishes it from other similar floods in Leh and Pakistan (Houze et al. 2017).

After a decade since the Uttarakhand flood, a similar devastating event occurred during July 7th to 11th, 2023, primarily impacting the Indian state of Himachal Pradesh. Over these four days, the entire state received 223 mm of rainfall, which was 436% more than its climatological value (reference period 1971-2020). While the rainfall departure was most pronounced over eastern Himachal Pradesh (861% of its average value), the total precipitation during these days was highest over the southern part of the region. The sustained rainfall led to the overflowing of major rivers, road blockages, landslides, and associated damages, resulting in the loss of approximately 72 lives and 7850 million Indian rupees worth of property (IMD Press Release titled "Unprecedented Rainfall in Himachal Pradesh for the Period 07.07.2023-11.07.2023 Brief Write Up". Shimla, 2023). In one of the few studies conducted on this event, Gupta et al. (2024) concluded that the heavy precipitation was primarily caused by multi-day low-pressure and convergence over the area. However, they noted that antecedent soil moisture contributed to the flood by reducing the infiltration rate. Another study proposed similar dynamics to the Uttarakhand flood, whereby the interaction between an eastward-propagating mid-tropospheric trough and monsoonal low played a substantial role (Raghuvanshi and Agarwal 2024). The analysis further emphasised the importance of Rossby Wave breaking, which allowed subtropical stratospheric air to encroach upon the equatorial troposphere.

Interestingly, a few recent studies have shed light on the similarities of broad-scale atmospheric circulation patterns between the July 2023 Himachal Pradesh and June 2013 Uttarakhand floods (Gupta et al. 2024; Raghuvanshi



and Agarwal 2024). These studies have provided a broad overview of the atmospheric precursors to NIS floods but lacked detailed investigation. For instance, both the abovementioned studies reported that the upper-level meridional wind divergence, caused by the southward intrusion of midlatitude westerly winds, is a common factor for the June 2013 and July 2023 flood events. However, whether that meridional wind divergence over NIS resulted from zonal wind convergence from both the eastern and western side or just due to the winds from the western boundary remains unclear. The origin of air-masses that intrude southwards causing divergence in the upper levels and atmospheric water sources which resulted in those two extreme rainfall events are unidentified until now. Additionally, most of the NIS flood studies rely on composite analysis, which is an effective way to reveal common factors responsible for various floods, but cannot explain the uniqueness between individual flood cases. A thorough investigation into individual flood events can identify targeted areas of model improvement for better flood forecast. To address the above-mentioned open scientific questions, we used the Lagrangian parcel tracing algorithm TRACMASS (Döös 1995; Aldama-Campino et al. 2020) along with Eulerian maps of relative vorticity at 850 hPa, integrated water vapour transport, wind speed and divergence at 200 hPa. This study, for the first time, traces the origin of air masses responsible for upper-level wind divergence during the June 2013 Uttarakhand and July 2023 Himachal Pradesh flood events. In addition, atmospheric moisture trajectories are also employed to identify and quantify the atmospheric water sources and pathways responsible for the extreme rainfall that caused these two devastating floods.

2 Data and methods

The daily data, computed from the hourly means, from ERA5 reanalysis has been used in this study to analyze the precipitation, relative vorticity at 850 hPa, Integrated Vapour Transport (IVT), wind speed and wind divergence at 200 hPa (Hersbach et al. 2020). The spatial resolution of the ERA5 data is 0.25°. The IVT is defined as

$$IVT = \sqrt{\left(\frac{1}{g} \int_{sfc}^{TOA} qudp\right)^2 + \left(\frac{1}{g} \int_{sfc}^{TOA} qvdp\right)^2}) \quad . \tag{1}$$

In equation 1, sfc indicates surface and TOA is Top of the Atmosphere model level. The specific humidity is denoted as q. The zonal and meridional wind velocities are given by u and v respectively. The acceleration due to gravity is g and dp represents pressure level thickness. The IVT has units in kg m⁻¹ s⁻¹. The 0.1° GPM-IMERG satellite daily resolution data is used to validate the precipitation obtained from the

ERA5 reanalysis (Huffman et al. 2020). Anomalies of different fields during the extreme rainfall events of June 2013 and July 2023 are calculated by subtracting the daily means from 1991 to 2010. A 20 year climatology period was chosen to exclude the study years, 2013 and 2023. This exclusion helps provide a clearer signal of the events when calculating anomalies. However, our results remain robust when using a 30 year climatology as well (results not shown). Note that hourly data (not daily) of specific humidity, surface pressure, and horizontal wind velocities at 137 vertical level are taken from ERA5 reanalysis to calculate atmospheric air and water transport. These transport fields are then used by a Lagrangian trajectory model named TRACMASS to compute atmospheric air and water trajectories. TRACMASS is a highly efficient and precise tool designed to compute Lagrangian trajectories. Initially introduced by Döös (1995), it has undergone continuous upgrades to improve its capabilities. TRACMASS utilizes an analytical solution to a differential equation to determine the trajectory path within each model grid box. This equation is based on the mass transport through the faces of a grid box, and the solution obtained is unique. As a result, trajectories can be computed both forward and backward to return exactly to their original positions. This two-way tracing capability of TRACMASS is a crucial feature for identifying the origins of water or air masses. In the present study, TRACMASS simulated trajectories used a stepwise-stationary scheme. This scheme linearly interpolates the calculated atmospheric air and water flux fields between two successive hourly data using intermediate time steps (here it is 3). Thus the Lagrangian model time step is 20 min. By assuming that the computed flux field remains constant during intermediate time steps, an exact solution of the differential equations can be found.

Lagrangian tracking model TRACMASS has been widely utilized in numerous studies to trace the movement of air and water transport (Döös et al. 2008; Berglund et al. 2021, 2022; Kjellsson and Döös 2012). In this study, we applied TRACMASS to understand the interaction between subpolar and subtropical jet streams and to identify the origin of the air masses responsible for upper-level wind divergence during extreme rainfall events in North India. A recent study by Dey et al. (2020) used TRACMASS to calculate the atmospheric trajectories of actual water masses (in kg/s), instead of humid air, using a three-dimensional atmospheric water mass flux field. These water trajectories can be interpreted as stream tubes which are impermeable and carrying atmospheric water from its source to destination. This adaptation enabled us to trace extreme precipitation events over NIS back to their evaporation sources, thereby identifying the origins of the atmospheric water responsible for these extreme rainfall events. The calculation of air trajectories also are stream tubes with the units kg/s of air. A detailed description of the Lagrangian trajectory model TRACMASS can be found in Döös et al.



(2017) and the derivation of atmospheric water transport and its validation is presented in Dey et al. (2020). The atmospheric air and water circulation pathways in the present study is identified by constructing a parcel position probability ($P_{i,j}$) map following Van Sebille et al. (2018):

$$P_{i,j} = \frac{P_{i,j}^c}{\sum P^c} \times 100\% \quad , \tag{2}$$

where $P_{i,j}^c$ is the trajectory crossing counts at a particular longitude (i), latitude (j) grid box and P^c denotes total number of trajectory crossing counts for all the grid boxes. The unit of $P_{i,j}$ is in % per horizontal grid box. The sum over all $P_{i,j}$ is thus 100%.

3 Results

3.1 Synoptic settings prior to extreme rainfall events over North Indian Subcontinent

3.1.1 Rainfall

The spatial distribution of daily accumulated ERA5 and GPM-IMERG satellite observed rainfall and its average over NIS (27°N–36°N, 72°E–83°E) for June 2013 and July 2023, along with the daily rainfall climatology is shown in Fig. 1. The area-averaged rainfall from ERA5 reanalysis shows good agreement with the GPM-IMERG satellite observation with notable differences

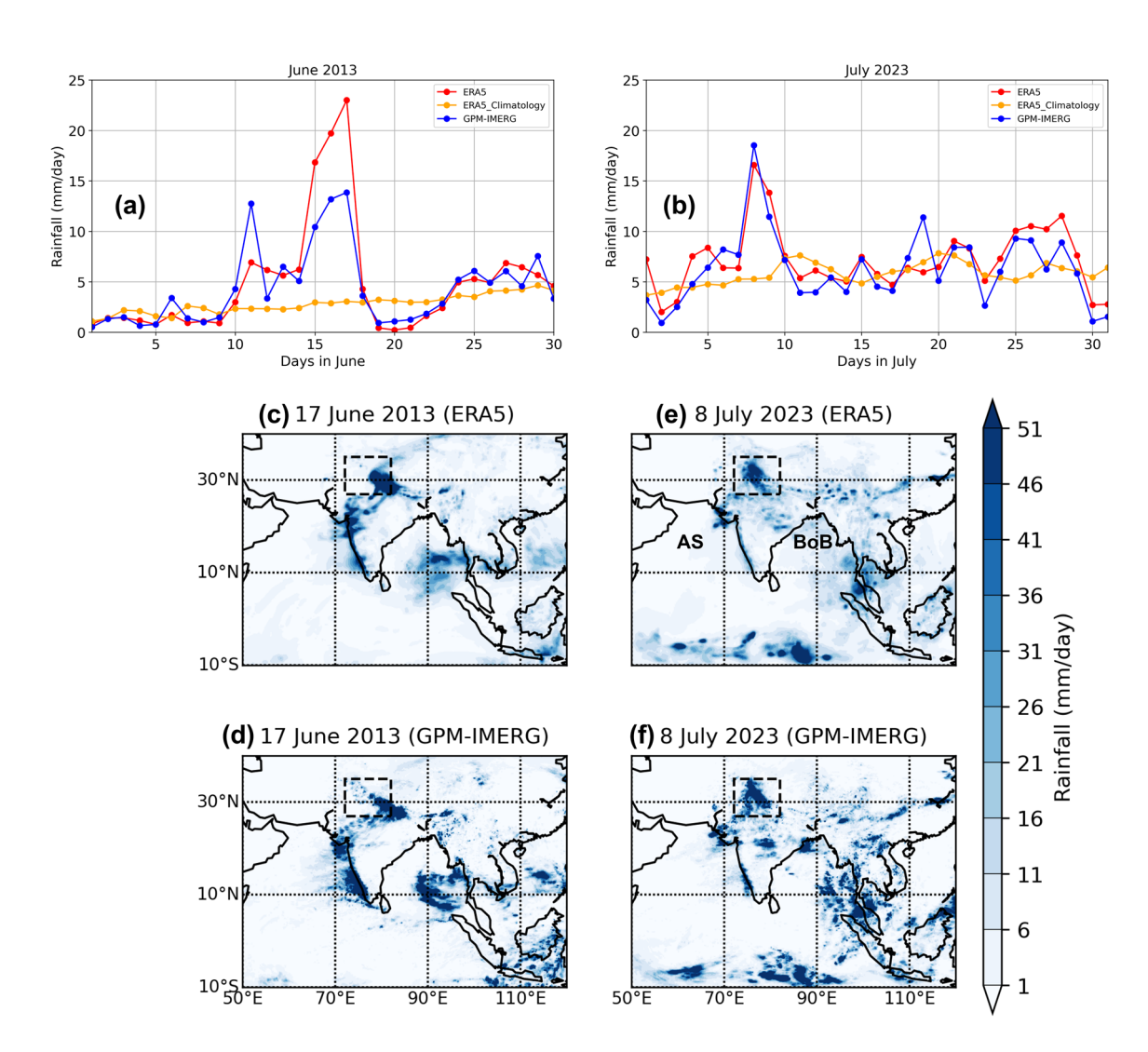


Fig. 1 Time series of daily accumulated precipitation (mm/day) averaged over North Indian Subcontinent (27°N–36°N, 72°E–83°E) during (a) June 2013 and (b) July 2023, along with the ERA5 daily accumulated rainfall climatology (orange line). The climatology is based on data from 1991 to 2010. The spatial rainfall distribution on 17th

June 2013 and 8th July 2023 from ERA5 reanalysis (**c**, **e**) and GPM-IMERG observation (**d**, **f**). The black dashed box represents North Indian Subcontinent in which the rainfall is averaged. Locations of the Arabian Sea (AS) and Bay of Bengal (BoB) are also shown



in magnitude (Fig. 1a, b). The correlation coefficient between the ERA5 and GPM-IMERG rainfall time series averaged over the NIS domain for June 2013 is 0.89 with a root mean square error of 2.76 mm. The daily rainfall evolution of June 2013 reveals (Fig. 1a) that the precipitation over NIS starts to enhance (departure from the climatological condition) from 10th June onwards and reaches its peak on 17th June. The highest daily accumulated rainfall recorded by GPM-IMERG on 17th June 2013 at a particular grid point (80.45°E and 29.35°N) over NIS domain is 226 mm. ERA5 reported 292 mm of rain on the same day, substantially higher than the observed satellite data. In this regard it is important to mention a study by Baudouin et al. (2020) which cross validated 20 gridded precipitation datasets and concluded that ERA5 reanalysis offers best rainfall estimate as compared to the satellite products. ERA5 was also used by Vellore et al. (2020) to study the extreme precipitation event of June 2013, as it accurately captured the sub-synoptic circulation variability. Note that as the spatial resolution of the GPM-IMERG (0.1°) and ERA5 (0.25°) data is not the same, the grid point location, in these two datasets, featuring the daily accumulated maximum rainfall will likely be different. During July 2023, the NIS average rainfall time series shows (Fig. 1b) that 4th July 2023 onwards the precipitation starts to deviate from its climatological conditions and hits maximum departure on 8th July 2023. The peak rainfall events on 17th June 2013 and 8th July 2023 are picked up by both the reanalysis and observed satellite data. The root mean square error between ERA5 reanalysis and GPM-IMERG satellite derived rainfall time series (Fig. 1b) during July 2023 is 2 mm with a correlation coefficient of 0.86. The ERA5 reanalysis-derived 103 mm of highest daily accumulated rainfall at a grid point (76.25°E and 31.75°N) within the NIS region is recorded on 8th July 2023. This is notably lower than the satellite observation of 230.5 mm on the same day.

The spatial rainfall pattern on the maximum rainfall days (Fig. 1c, f) indicates that the June 2013 event was concentrated on the southeast quadrant of the chosen NIS box while the July 2023 extreme rainfall was well spread across the box. It also confirms that the ERA5 data is able to reproduce the spatial distribution of extreme rainfall on those particular days when comparing with the GPM-IMERG observation. It is noteworthy that during the June 2013 case, ERA5 seems to spread the heavy precipitation over a wider area while GPM-IMERG has a region of lighter rain to the northwest of the NIS region. A high spatial and temporal correlation between the reanalysis and observation gave us the confidence to use ERA5 reanalysis for further analysis (Baudouin et al. 2020).

3.1.2 Relative vorticity and integrated vapour transport

To identify the role of lower level atmospheric dynamics on the peak rainfall days i.e. 17th June 2013 and 08th July 2023 we have investigated the 850 hPa relative vorticity and whole atmospheric column integrated vapour transport. As 850 hPa pressure level does not exist in the Himalaya or over the Tibetan Plateau, we have masked out regions where the surface pressure is less than 850 hPa. The vertically integrated water vapour transport has been taken directly from ERA5. The ERA5 calculates vertical integral on model levels which follows terrain. This ensures that in the mountainous regions no values below the orography are taken for vertical integration. The column-integrated vapour transport is primarily dominated by the lower atmospheric levels as 90% of the atmospheric moisture is concentrated below 500 hPa (Peixoto and Oort 1992; Dey and Döös 2019). Prior to the 17th June 2013 rainfall event, two closed cyclonic systems (concentrated high values of positive relative vorticity, counterclockwise spin) appear to be present over the northern Indian Ocean, one in the Arabian Sea and another over the Bay of Bengal (Fig. 2).

These cyclonic systems are indicative of monsoon lowpressure systems as noted earlier by Houze et al. (2017). The two cyclonic systems and corresponding atmospheric vapor transport starts to move inland towards the Indian peninsula and merge together by 16th June 2013, a day earlier than the peak rainfall day (Figs. 2a, e and 3a, e). The results show that atmospheric water vapour transport is influenced by the presence of synoptic closed cyclonic systems, which move toward NIS prior to the above-normal rainfall on 17th June 2013. The study by Vellore et al. (2020) demonstrated that cyclonic vorticity can be sustained through the influence of an equatorward-intruding trough located well south of 20°N. The vapour transport also revealed a dominant in-land pathway for the 2013 event (Fig. 3d, f). We will examine, using Lagrangian trajectories, in later sections the origins of moisture and their pathway in order to ascertain this.

The lower-level atmospheric circulation prior to the 8th July 2023 rainfall event is quite different than the 2013 episode. The monsoon trough is active over the Bay of Bengal and Arabian Sea southward of 20°N, instead of closed cyclonic circulations (Fig. 4).

The results indicate that due to the active monsoon trough the vapour transport band, which causes above-normal rainfall over NIS, shifted southward from its normal position and stretches now from the Arabian Sea to the Bay of Bengal (Fig. 5).

The vapour transport pathway is found to be more dominant over the ocean for the 2023 episode, a result in contrast to the 2013 event in which in-land moisture pathway is noted to be important. Separation of the wind and



230 Page 6 of 17 D. Dey et al.

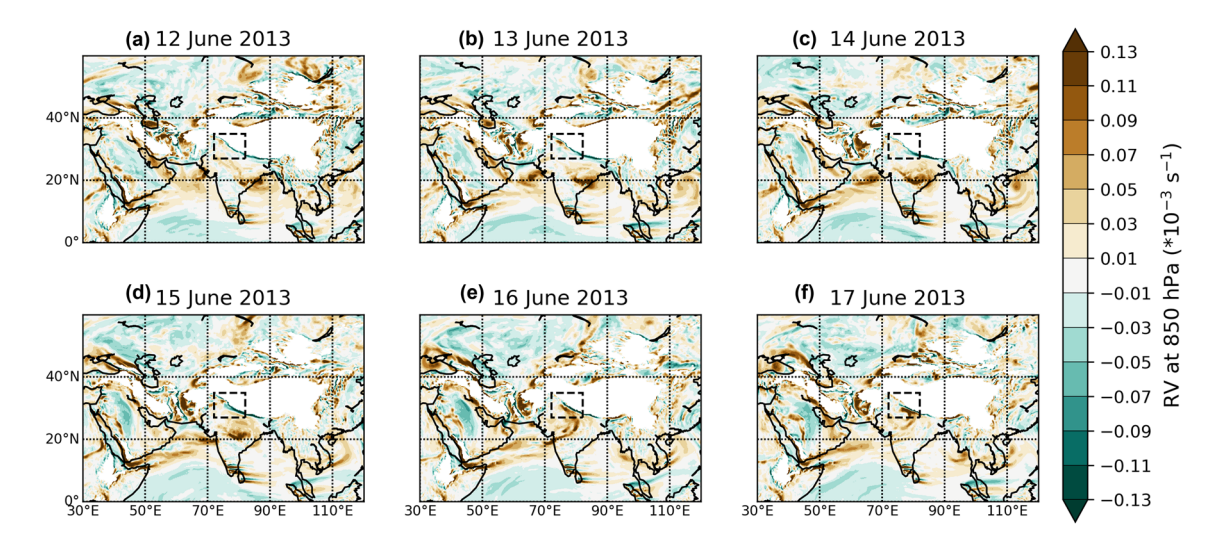


Fig. 2 ERA5 relative vorticity (RV) at 850 hPa (unit is in s⁻¹) from 12th June 2013 to 17th June 2013. Positive values indicate counter-clockwise spin. While the negative values typically means clockwise spin. The black dashed box represents North Indian Subcontinent. We

have masked out the regions where surface pressure is less than 850 hPa. Two closed cyclonic systems (high values of positive relative vorticity) are noted to be present over the northern Indian Ocean prior to the 17th June 2013 extreme rainfall

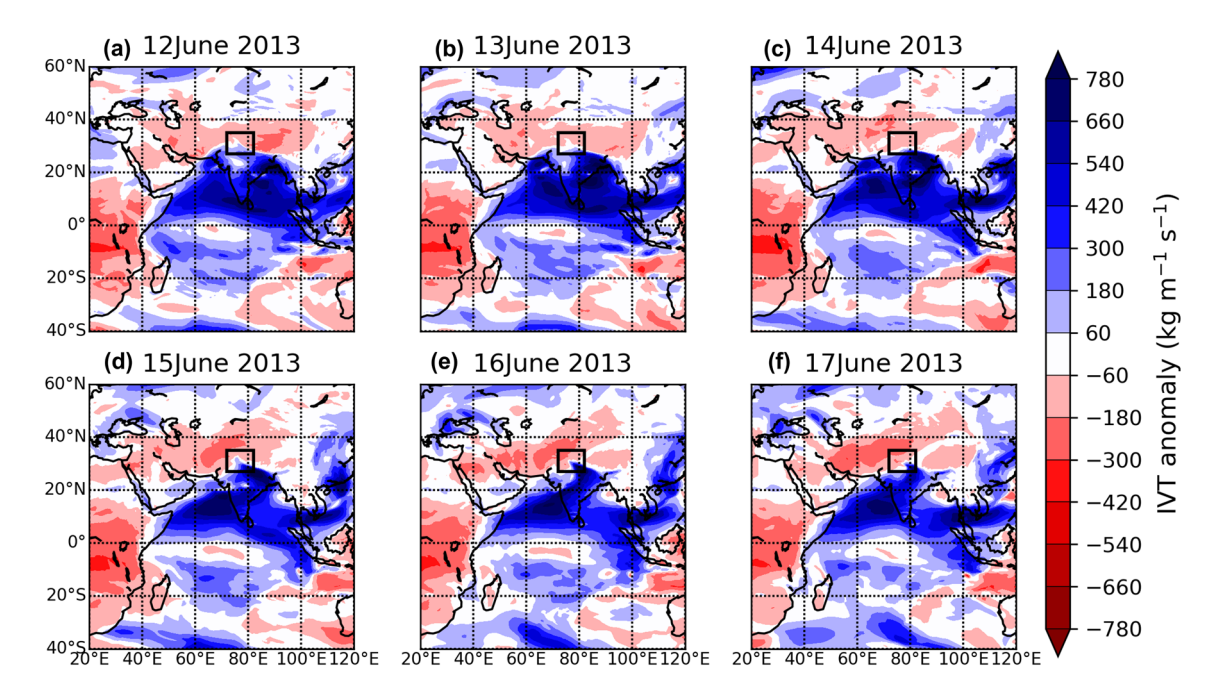


Fig. 3 ERA5 Integrated Vapour Transport (IVT) anomaly (unit: kg m⁻¹ s⁻¹) from 12th June 2013 to 17th June 2013. IVT anomalies are relative to climatology over 1991–2010. The positive values indicate above average water vapour transport while negative value represents

lower-than-normal transport of water vapour. The black color box represents North Indian Subcontinent. The anomalously high atmospheric vapour transport shows a dominant in-land pathway prior to the 17th June 2013 rainfall

moisture fields further reveals that it is the low-level wind variability rather than moisture variability that controls the integrated vapour transport during these two events, a clear dominance of atmospheric dynamics over thermodynamics (see the supporting information Fig. S1).

3.2 Upper-level divergence and air tracing

Extreme precipitation events over NIS during the monsoon period are often found to be associated with the interactions between monsoon synoptic systems and extratropical circulations (Vellore et al. 2016; Hunt et al. 2021). The



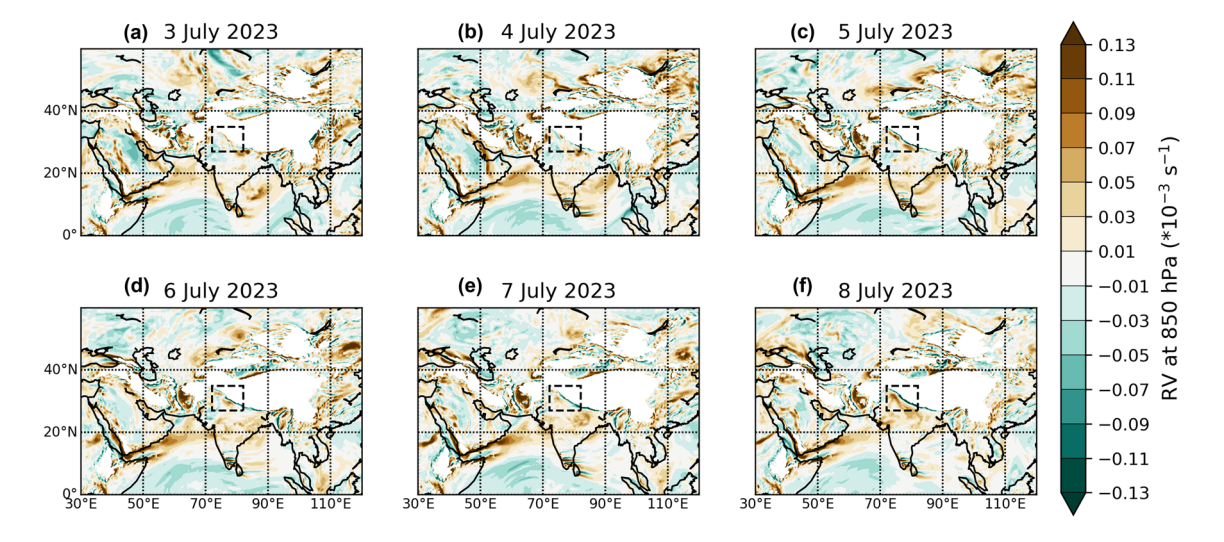


Fig. 4 Same as Fig. 2 but during 3rd July 2023-8th July 2023. A prominent band of high positive relative vorticity stretches between the Arabian Sea and the Bay of Bengal preceding the 8th July 2023 extreme rain, particularly noticeable from 3rd July 2023 to 6th July 2023

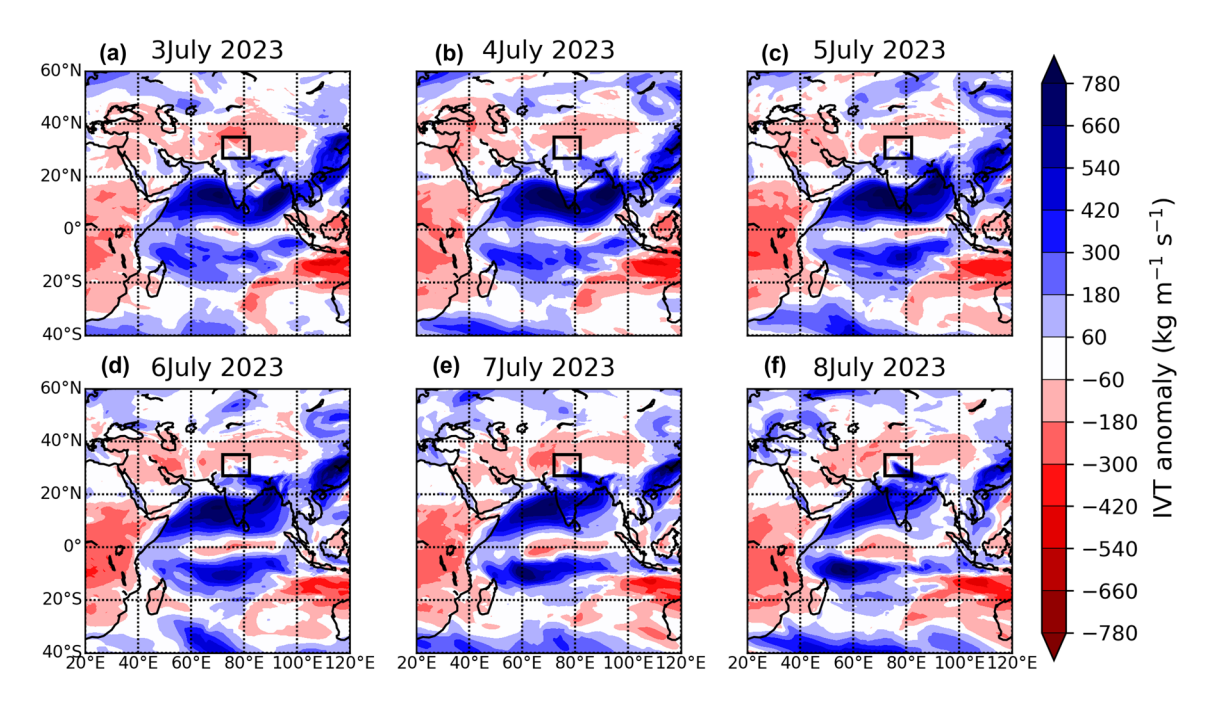


Fig. 5 Same as Fig. 3 but during 3rd July 2023-8th July 2023. The atmospheric vapour transport pathway is notably prominent over the Bay of Bengal from 3rd July 2023 to 6th July 2023

extratropical influence in many cases arises from troughs in the mid-latitude subtropical westerly jet stream that intrude southward towards NIS and create upper-level divergence at the entrance to the downstream jet streak, causing anomalous ascent by ageostrophic effects.

To understand the role of upper-level winds on the June 2013 and July 2023 rainfall episodes we have plotted largescale wind speed pattern and the divergence at 200 hPa averaged over NIS in Figs. 6 and 7 respectively. Before the 17th June 2013 peak rainfall, a trough is created on the subtropical jet stream between 60°E-90°E which starts to migrate southward from 13th June 2013 onwards (Fig. 6c, f).

A similar kind of trough is also noted prior to the July 2023 rainfall event. The trough in the mid-latitude subtropical westerly jet stream starts to move southwards on 4th July 2023 from its original position towards NIS (Fig. 7c, f).

It is interesting to note that for both the events the trough incursion is not directly occurring over the NIS flood box but



230 Page 8 of 17 D. Dey et al.

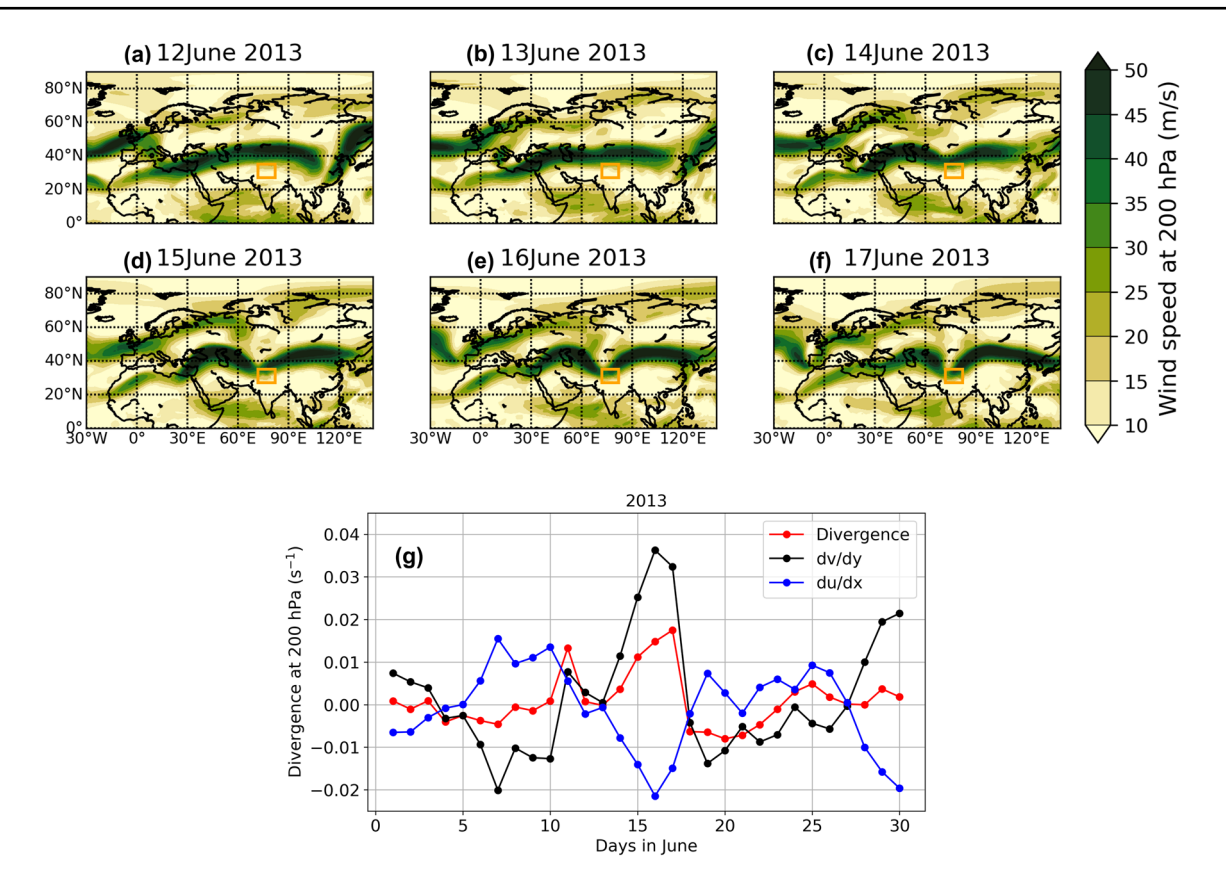


Fig. 6 Upper panels (**a–f**): ERA5 wind speed at 200 hPa (m/s) from 12th June 2013 to 17th June 2013. The orange box represents the North Indian Subcontinent study region (27°N–36°N, 72°E–83°E). Southward migration of the subpolar jet stream and interaction with

its subtropical counterpart can be noted from 14th June 2013 onward. Lower panel (g): ERA5-derived divergence at 200 hPa (s⁻¹) averaged over North Indian Subcontinent during June 2013

west of it (Figs. 6 and 7). The wind outflow over NIS due to the westward situated upper level trough creates divergence. Interestingly an independent study on the evolution, seasonality and impacts of western disturbances (Hunt et al. 2018b) also revealed that the upper-level divergence enhances to the east of the trough which in their study was created by winter time western disturbances. Due to the trough incursion the upper-level divergence shows enhancement from 13th June to 17th June 2013 and 04th July-08th July 2023 (Figs. 6g and 7g). It is noteworthy that the rainfall also shows amplification during these times (Fig. 1). The close association between upper-level divergence and rainfall strengthens the argument put forward in earlier studies that the creation of divergence in the upper levels of the troposphere is responsible for extreme rainfall over NIS (Joseph et al. 2015; Houze et al. 2017; Hunt et al. 2018b; Vellore et al. 2020). A study on the causes of the June 2013 flood event demonstrated that cyclonic vorticity on the right flank of the upper-level potential vorticity (PV) anomaly (trough) facilitates the development of a deeper mesoscale convergence zone, where prominent vertical synchronization of positive PV advection and extreme rainfall occur (Vellore

et al. 2020). In addition, interaction with the steep mountains of the region as the upper-level divergence centre approaches it further increases the ascent via orographic uplift, increasing the likelihood of heavy rainfall there (Hunt et al. 2018b).

A detailed investigation reveals that the increase in divergence arises due to latitudinal variation of meridional velocity (i.e., higher meridional wind at the northern wall of the NIS box as compared to its southern wall) as shown by black line in Figs. 6g and 7g which ultimately results from zonal wind convergence (blue line in Figs. 6g and 7g). The upper-level wind speed during these two events hints that the trough in the subtropical jet stream forms in conjunction with southward migration of the subpolar jet stream which can be seen between 50°N–60°N and 60°E–90°E (Figs. 6 and 7). This observation points towards a possible interaction between the subtropical and subpolar jet stream.

To explore the nature of the connectivity between the subtropical and polar jet streams we have traced southward moving air 10 days backward in time from the days of peak rainfall where the subpolar jet stream interacts with subtropical jet stream (Fig. 8). The air parcel position probability map (calculated using equation 2), which indicates



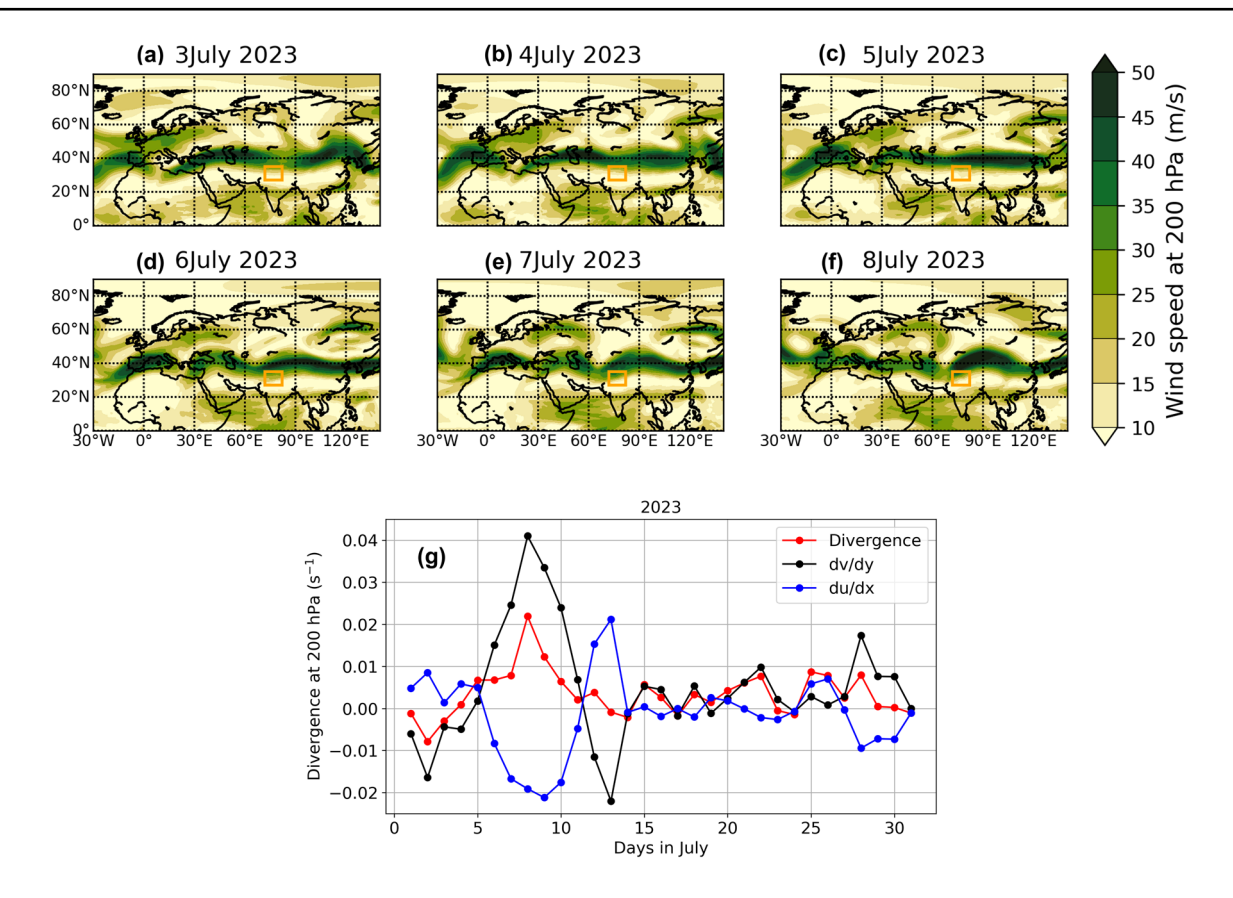


Fig. 7 Same as Fig. 6 but for July 2023. Southward movement of the subpolar jet stream and its interaction with subtropical jet stream can be seen from 6th July 2023 onward

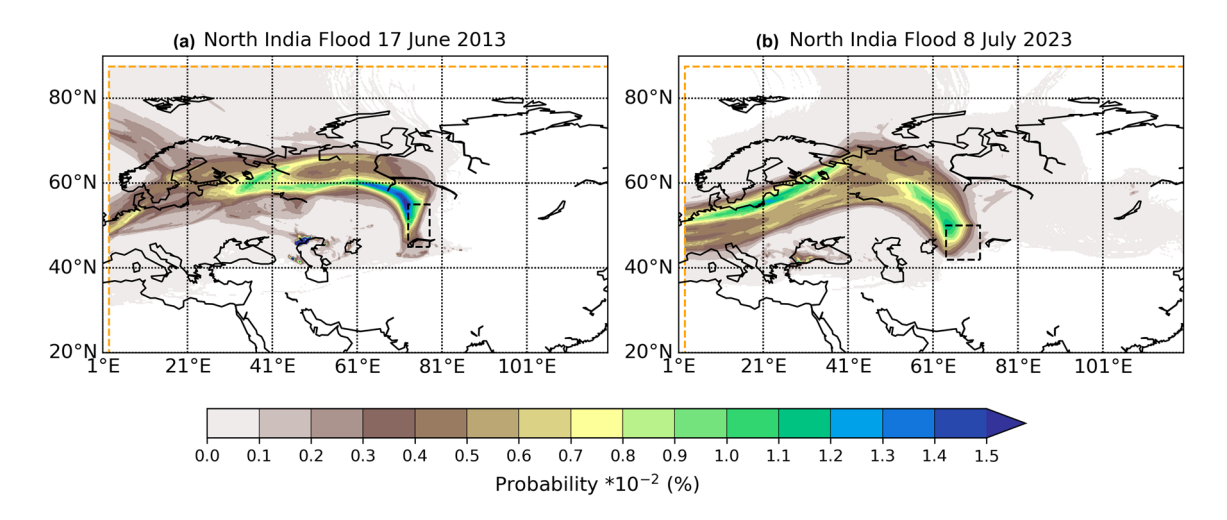


Fig. 8 Air parcel position probability map (%). These are constructed using 10-day backward-tracing Lagrangian air parcels which initially move southward along ≈ 148 hPa-296 hPa pressure levels over (a) 73°E-78°E, 45°N-55°N during 17th June 2013 and (**b**) 64°E-72°E,

42°N-50°N during 8th July 2023. The black dashed boxes represent the areas mentioned above. The orange dashed lines are the air trajectory termination boundaries. High values indicate dominant air pathways

air transport pathways, clearly affirms that the subpolar jet stream, situated approximately between 50°N-60°N, moves southward towards the subtropical jet stream. Lateral influence of the subpolar jet stream possibly results in trough creation along the subtropical jet stream prior to the extreme rainfall days.

The upper-level meridional wind divergence, which is responsible for extreme rainfall, results from the zonal wind



230 Page 10 of 17 D. Dey et al.

convergence (discussed earlier) and needs to be investigated further for more detailed understanding. For this purpose, the air parcels which travel northward along $\approx 148 \text{ hPa-}296 \text{ hPa}$ over the NIS box are tracked backward in time for 10 days (Fig. 9).

The results show that during the June 2013 episode, the northward moving air mostly arrives with the upper level westerlies (Fig. 9a). Furthermore, it indicates that air from the Bay of Bengal and Arabian Sea also contributes to the meridional divergence by merging with the mid-latitude westerly winds. We will later examine the pressure along the trajectories to explain a complete 3-D structure of the pathways. However, air transport routes tell a different

story for the July 2023 episode (Fig. 9b). The pathways of upper-level air transport seems to be dominant over the Indo-Gangetic plains, indicating a higher contribution from the easterly winds than the mid-latitude westerlies. Additionally, air pathways contributing to the upper-level divergence in the flood region originate over the Arabian Sea and closely resemble the lower tropospheric cross-equatorial monsoonal flow. This observation suggests that the lower tropospheric flows are ascending towards higher levels. To establish this, we have plotted air pressure along trajectory pathways (Fig. 10).

It can be seen from Fig. 10b that the air parcels originating in the boundary layer over western equatorial

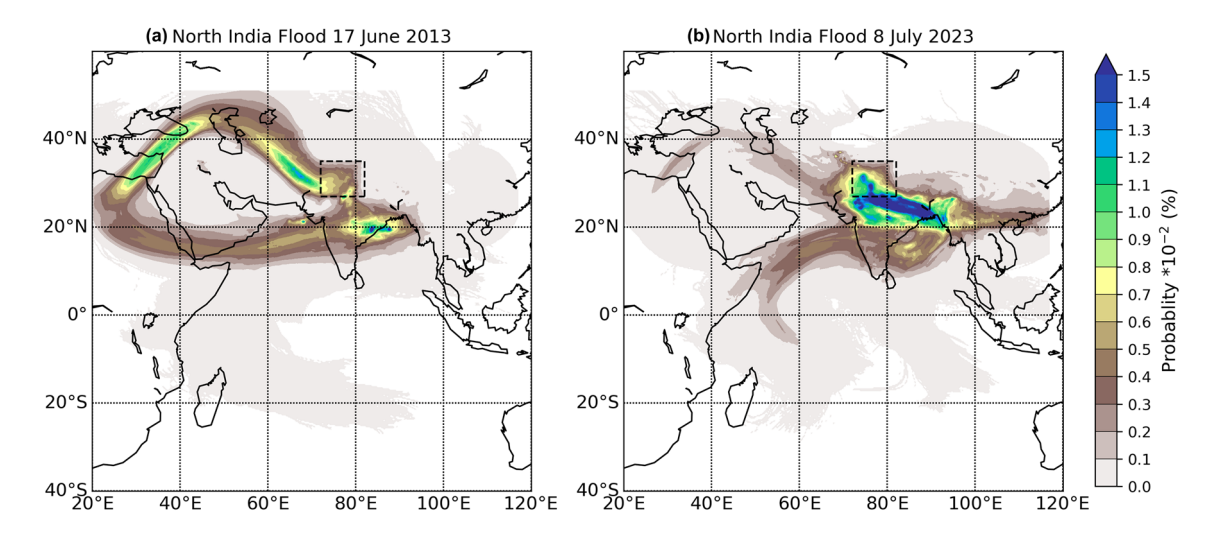


Fig. 9 Air parcel position probability map (%). These are constructed using 10-day backward tracing Lagrangian air parcels which initially move northward along≈ 148 hPa−296 hPa pressure levels over North

Indian Subcontinent $(27^{\circ}N-36^{\circ}N, 72^{\circ}E-83^{\circ}E$ and are represented by a black dashed box) (a) during 17th June 2013 and (b) during 8th July 2023

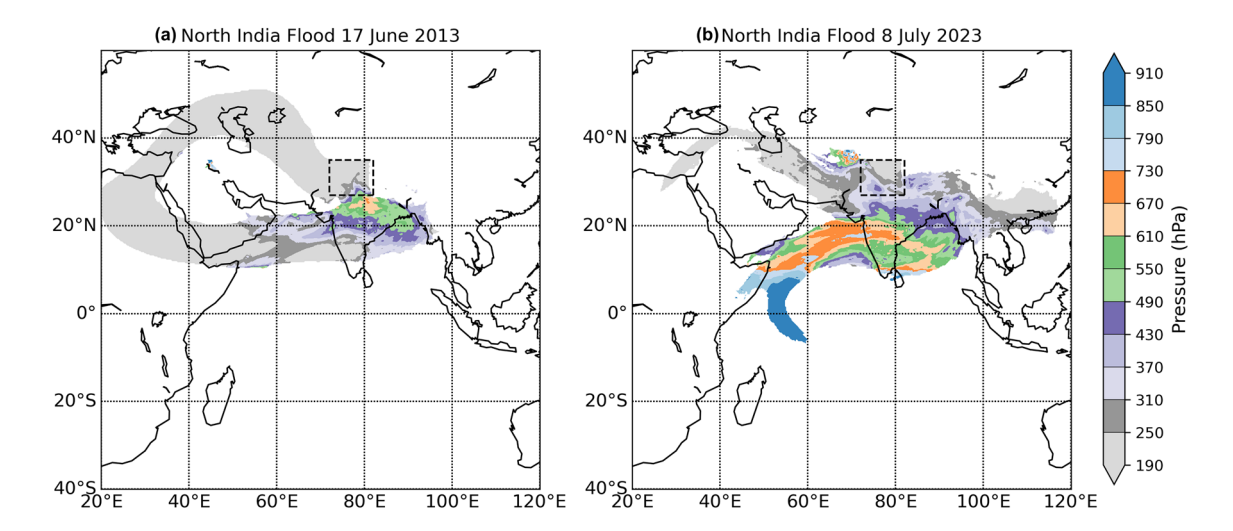


Fig. 10 Air pressure along trajectory pathways(hPa). These are constructed using 10-day Lagrangian air parcels which initially move northward along ≈ 148 hPa-296 hPa pressure levels over North

Indian Subcontinent (27°N–36°N, 72°E–83°E, represented by the black dashed box) during (a) 17th June 2013 and (b) 8th July 2023



Indian Ocean are gradually ascending as they cross the Arabian Sea and further as they cross the Bay of Bengal. These air parcels then merge with the upper-level easterly winds (part of the tropical easterly jet) along the Indo-Gangetic plains and flow towards the flood region. The role of the subtropical westerly jet in the upper levels is less dominant for the 8th July 2023 rainfall event. The air pressure along trajectories reveal that prior to the 17th June 2013 rainfall event, the relatively lower-level air parcels over the Bay of Bengal and land areas ascend into the tropical easterly jet and are advected over over the Arabian Sea before traversing the Red Sea and merging with the mid-latitude subtropical jet stream (Fig. 10a). The upper-level subtropical westerly jet is more dominant for the 17th June 2013 rainfall spell. Zonal wind convergence can occur in two scenarios: (i) higher eastward (westerly) zonal wind at the western wall than the eastern wall of the North India box or (ii) high westward (easterly) wind at the eastern wall and lower eastward (westerly) wind at the western boundary. In summary, the first scenario occurs when strong westerly winds are present and easterly winds give rise to the second scenario. The Lagrangian air tracing proves that for the June 2013 event the zonal wind convergence occurs due to the westerly winds while the easterly winds are responsible for convergence during the July 2023 event.

3.3 Evaporative sources of the extreme rainfall

Although the upper-level wind pattern creates favourable conditions for extreme rainfall, it is the lower levels that provide the required moisture (Hunt et al. 2018a, 2021). To trace the origins of atmospheric moisture for the two cases of NIS floods, we have traced precipitation backwards in time for 30 days from the flood region until it reaches its evaporative sources. For both cases, the local evaporative sources (local recycling) play an important role in providing water for extreme rainfall (Fig. 11).

However, there are distinct differences in net evaporative sources. A narrow channel of atmospheric moisture over the western Indian Ocean concentrated between 20°S-20°N, 40° E-70°E and the Persian Gulf provides most of the oceanic evaporative sources for the 17th June 2013 event (Fig. 11a). Instead, for the 8th July 2023 rainfall event, the oceanic sources of evaporation are originating from two channels south of 20°S, one from the southeast and another from the southwest (close to Madagascar) and then spread all along the pathway of the lower-tropospheric monsoon circulation in the western Indian Ocean as shown in Fig. 11b. It is important to note, during the June 2013 case the in-land evaporative sources are greater than those in the July 2023 episode, particularly from eastern peninsular India, which closely matches with the Eulerian integrated vapour transport maps presented in Figs. 3 and 5. To explore the possible reason behind a greater in-land source of moisture for

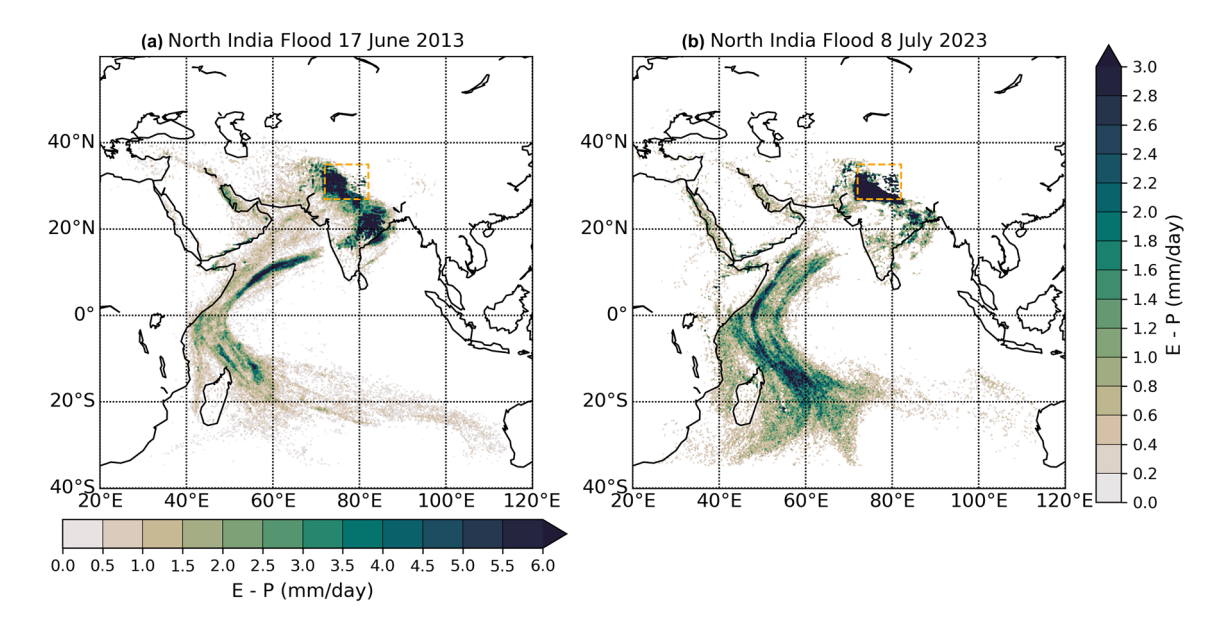


Fig. 11 Net evaporative sources (mm/day) responsible for the (a) 17th June 2013 and (b) 8th July 2023 North Indian Subcontinent floods. Calculations consider all the atmospheric water trajectories that reached the surface after backward tracing of precipitation from

the North Indian Subcontinent box. The orange dashed box indicates the North Indian Subcontinent region from which the backward trajectories are initialised. Note that the colour scale is different in each case



the June 2013 case, we have mapped the residence time of atmospheric moisture at their evaporative locations (see supporting information Fig. S2). It shows that the in-land evaporation of surface waters occurred mostly 4 days prior to the extreme rainfall in Uttarakhand on 17th June 2013. The rainfall time series in Fig. 1a shows a spike on 11th June 2013. We speculate that that this rainfall saturated the ground, then later it evaporated by 14th June 2013 and contributed to the flood. The Bay of Bengal does not contribute actively as an evaporative source for either of the NIS floods studied here. The evaporative sources of extreme rainfall over the NIS has been identified when the backward water trajectories (precipitation) reached the surface again (evaporation). We have not further traced back that origin of surface evaporation. For the June 2013 case, the residence time of in-land moisture (see supporting information Fig. S2) indicates that it evaporated mostly 4 days prior to the extreme rainfall. Since we have not traced back that evaporation, it is possible that the synoptic closed cyclonic system over the Bay of Bengal deposited precipitation over eastern peninsular India 4 days earlier, which later evaporated and contributed to the extreme rainfall over the NIS. The integrated vapour transport anomaly map in Fig. 5 clearly hints towards higherthan-normal vapour transport over the Bay of Bengal during 2023 event. In order to understand this in more detail, we have mapped water transport pathways from the atmospheric moisture back trajectories (Fig. 12).

The Lagrangian results shows that atmospheric water paths over the Bay of Bengal are more prevalent for the July 2023 case than the 2013 event (Fig. 12b), a result similar to the Eulerian higher-than-normal vapour transport map in Fig. 5. It also indicates that the atmospheric water present

in the transport pathway is not originating from the Bay of Bengal. The dominant in-land water transport pathways during June 2013 are also evident in Fig. 12a but the closed cyclonic systems are not noticeable. To explain this, we have plotted the age of atmospheric water, which shows the time remaining for moisture to reach the extreme rainfall location in the NIS from each point along its trajectory (Supporting Information Fig. S3). Whether it was possible to observe a cyclonic system in water transport field depends on the location and timing of atmospheric moisture relative to the presence of cyclonic systems. Supporting Information Fig. S3a demonstrates that, 4 days prior to the extreme rainfall, the evaporated atmospheric moisture was mostly present along a channel stretching from the Arabian Sea to the NIS. The IVT in Fig. 3 also reveals that, 4 days prior (i.e., from June 14, 2013, onwards), the cyclonic systems could not be distinctly identified. The presence of closed cyclonic vorticity systems in relative vorticity field (Fig. 2), combined with their absence in IVT, indicates that the cyclonic systems were not directly carrying the moisture but were influencing its pathways.

4 Discussion and conclusion

Floods along with avalanches, debris flow and landslides are frequent hazards in the mountainous regions (Stäubli et al. 2018). The Indian Himalayan region is particularly vulnerable to such phenomena (Lindell et al. 2019; Dash and Punia 2019). During the Indian summer monsoon, the Indian Himalayan region experiences intense and sustained rainfall that sometimes leads to floods (Nagamani et al. 2024).

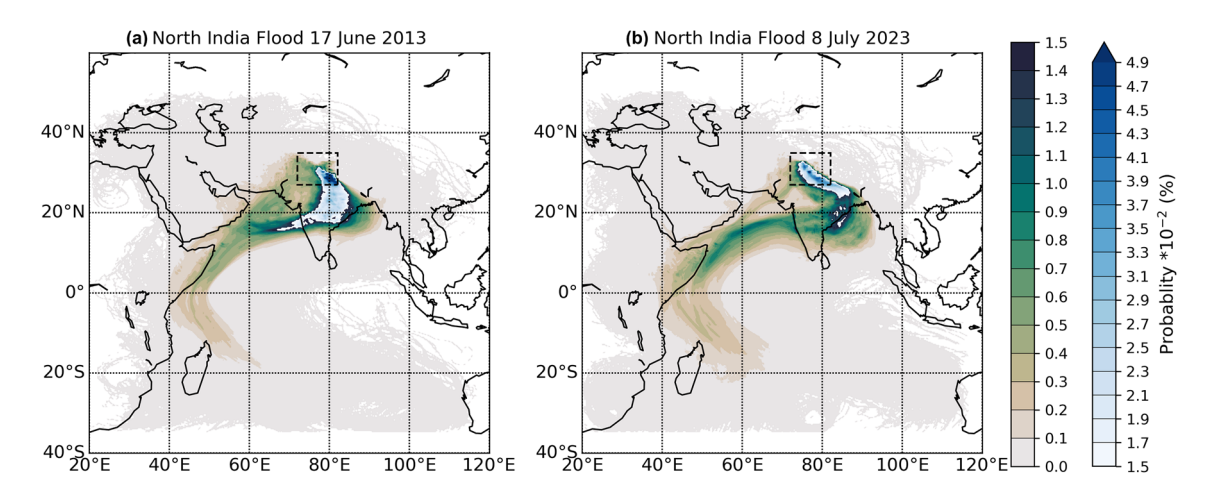


Fig. 12 Atmospheric moisture parcel position probability map (%). This has been calculated by considering all the atmospheric water trajectories that reached the surface after backward tracing of precipitation from the North Indian Subcontinent box (27°N–36°N, 72°E–83°E and represented by the black dashed box) for (a) the 17th June

2013 and (b) 8th July 2023 events. As the moisture parcels approach the target area they will start to concentrate. This will lead to high values of atmospheric moisture parcel position probability near the target region. To clearly visualize the pathways of ocean origin moisture parcels also we have used two different colour maps and scales



The Intergovernmental Panel on Climate Change (IPCC) unequivocally stated in their recent report that water-related hazards like floods will have increased damage and losses as the global warming level increases between 1.5°C and 3°C (Adler et al. 2022). Many scientific studies have also showed that the frequency of extreme events in the mountainous regions is increasing due to climate change (Baidya et al. 2008; Vogel et al. 2020). There is therefore an urgent need for the scientific community to identify the dynamical processes responsible for these mountain floods and to ensure these processes are correctly represented in the numerical models used for precipitation and flood forecasting.

Earlier meteorological studies on floods over the Indian Himalayan region have mostly comprised a broad overview of the large-scale atmospheric circulation pattern responsible for such events, without providing detailed information on the associated dynamical patterns. In the present study, we have used a combination of Eulerian maps and a Lagrangian parcel tracing algorithm, TRACMASS, to identify the air and water-mass sources and their pathways responsible for the June 2013 Uttarakhand and July 2023 Himachal Pradesh floods. By doing so we have elucidated the similarities and differences in the atmospheric circulation during these two flood case studies.

The results obtained from ERA5 reanalysis and GPM-IMERG observations show that, during the Uttarakhand flood, rainfall started to intensify from 13th June 2013 onwards and reached its peak on 17th June, while for the Himachal Pradesh flood, precipitation started to increase from 4th July 2023 and peaked on 8th July 2023. The presence and merging of two low pressure systems in the north Indian Ocean were found to be a main contributing factor for the 2013 flood event. These synoptic weather systems helped to create a channel of vapour transport from the Arabian Sea to NIS, which supplies moisture for extreme rainfall, resulting in flooding. In contrast, a southward shift of the monsoon trough and associated vapour transport over the Arabian Sea and Bay of Bengal was found to be important for the 2023 flood event.

Examination of the upper-level atmosphere during these two flood cases revealed southward incursion of the subtropical jet stream as a common factor, a result consistent with earlier studies (Gupta et al. 2024; Raghuvanshi and Agarwal 2024). Additionally, it has been noted that the incursion occurs on the west side of the flood area and not directly over it. A time series of upper-level divergence confirms that, due to the subtropical jet incursion on the west side of the flood area, meridional wind divergence accompanied by zonal wind convergence occurs directly over the floodhit location at upper levels. The strong correlation between upper-level divergence and rainfall time series confirms the role of southward intrusion of the subtropical jet stream in creating these two flood events.

Zonal winds mapped in the upper levels reveal a possible connection between the southward displacement of the subtropical jet stream and the subpolar jet. To confirm this, we back-traced upper-level air parcels which move southward with the subtropical jet. The back trajectories clearly demonstrate that southward movement of the subtropical jet stream is associated with southward movement of the subpolar jet. Detailed analysis of the pathways reveals the role of upper-level easterlies and ascending air from the lower level cross-equatorial monsoon flow to higher atmospheric levels in advance of the 2023 Himachal Pradesh floods. Moreover, we also found that key meridional divergence during the 2013 flood event was associated with the upper-level midlatitude westerly winds. Whereas, during the 2023 case, the upper level easterlies (with a relatively small contribution from westerlies) converged to produce the necessary meridional wind divergence.

The back-tracking of extreme precipitation during the two cases shows that in-land evaporation contributions are more substantial for the 2013 flood than that of 2023. Additionally, the western Indian Ocean was found to be the major non-local source for the Uttrakhand flood of 2013. For the 2023 flood, two evaporative channels starting close to Madagascar are identified as contributing to high rainfall across North India. The Bay of Bengal participates in these two extreme rainfall events only as the pathway for vapour transport, and not directly as a moisture source. The Lagrangian vapour transport maps closely resemble the corresponding Eulerian maps, in which in-land moisture transport is identified as a dominant factor for the Uttarakhand flood. In contrast, the north Indian oceanic moisture pathway is found to be important for the 2023 Himachal Pradesh flood. All the important findings of the present study are summarised schematically in Fig. 13. Note that the low level moisture laden flow from the evaporative source regions to the extreme rainfall locations is part of the monsoonal flow regime. Therefore, it is important to further investigate factors influencing the moisture transport pathways, such as the Southern Hemisphere Annular Mode (Dou et al. 2017), Freeze-Thaw cycles of the Tibetan Plateau (Zha and Wu 2025), El Niño-Southern Oscillation (Webster et al. 1998; Zhang et al. 2024) and other dynamic processes during extreme rainfall events.

In conclusion, the present study has revealed a new dynamical mechanism that leads to extreme rainfall over the foothills of Himalayas. Previous studies emphasised a role for the subtropical jet stream in the development of upper level divergence, associated with lower level convergence. Here, we further show the key role of subpolar jet stream in displacing the subtropical jet stream southwards, as an essential factor ahead of those devastating floods. We additionally emphasise that although the 2013 and 2023 floods over North India are associated with similar broad-scale atmospheric circulation, our detailed analysis reveals clear



230 Page 14 of 17 D. Dey et al.

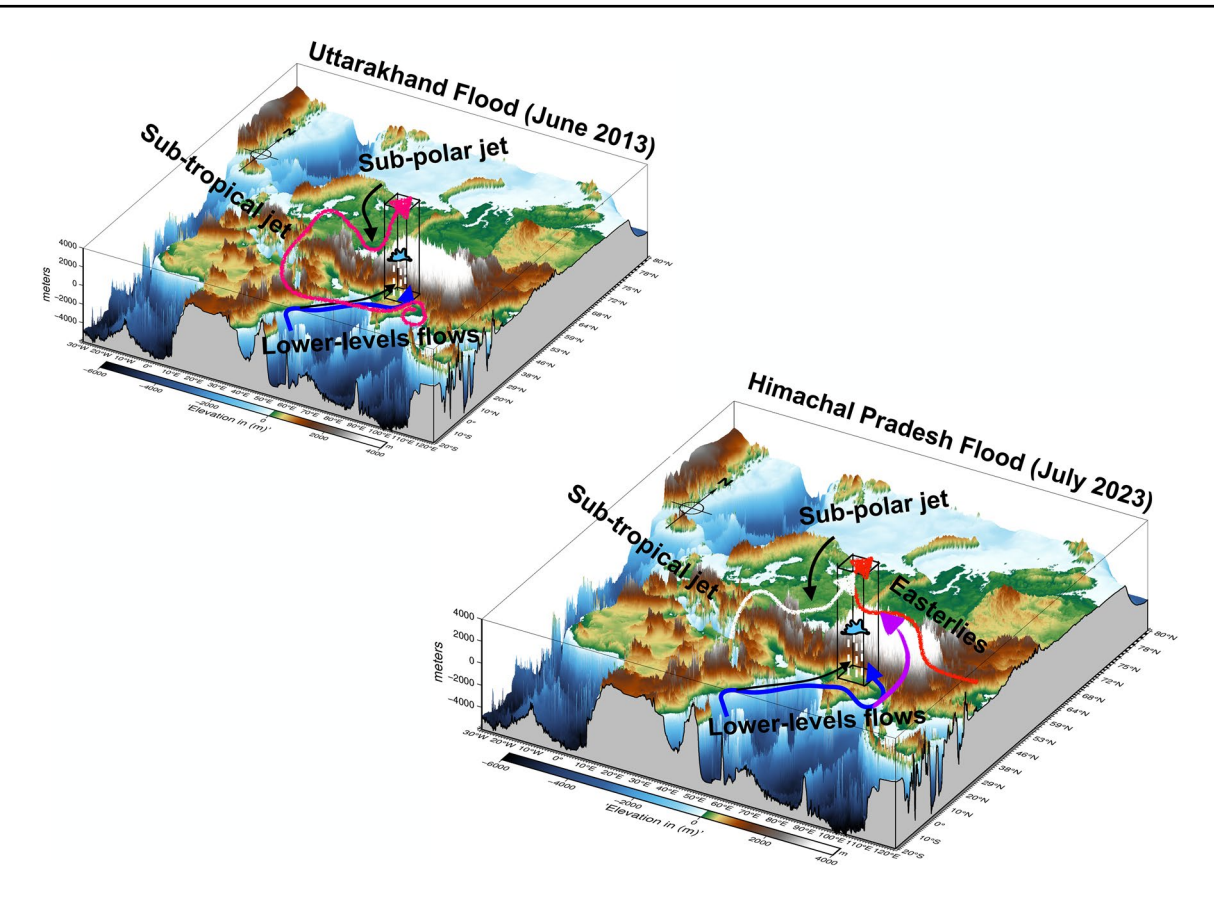


Fig. 13 Schematic representations of mechanisms responsible for the June 2013 Uttarakhand flood and July 2023 Himachal Pradesh flood. The white arrow represents the subtropical jet stream while the red arrow corresponds to upper-level easterly winds

differences in the synoptic details. We acknowledge that many questions still need to be answered, such as whether Rossby wave breaking plays a key role in southward movement of the jet streams, why the two cyclonic systems were present before the June 2013 event, the reasons for different moisture sources, and whether these are related to the location of subtropical and subpolar jet interactions. It is important to note that previous studies (e.g., Vellore et al. (2016, 2020)) have demonstrated the role of Rossby wave breaking (RWB) in the June 2013 event, highlighting its contribution to the southward displacement of jet streams and the equatorward movement of high PV air from higher latitudes. While the equatorward movement of high PV air can be a signature of RWB, it is not always indicative of it. High PV air can move equatorward without undergoing irreversible mixing-an important characteristic of RWB-particularly when jet stream undulations result from small-scale transient baroclinic waves, sudden stratospheric warming (Toptunova et al. 2025), Arctic amplification (Francis and Vavrus 2015; Geen et al. 2023) or other dynamic processes. A sophisticated PV-based tracking algorithm is useful to precisely detect RWB events (e.g., Tamarin-Brodsky and Harnik (2024)). However, since the present study did not employ such an algorithm, it cannot confirm whether RWB played a role in the formation of jet stream troughs during the June 2013 and July 2023 events. From a forecasting perspective, it would be insightful to further establish the sensitivity of North India floods to latitudinal position of the subpolar jet stream. The present study could accordingly be extended to include many more flood case studies, to determine whether interaction of the subpolar and subtropical jet streams is a more robust, and hence predictable, phenomenon. The upstream drivers of extreme monsoon rainfall identified here, specifically evaporation over the Indian Ocean at lead times of days-weeks, further indicates the potential for improved operational forecast skill. A valuable addition to the existing forecasting capabilities would be running TRACMASS on-line with a forecast model. The operational use of the TRACMASS algorithm can provide detailed insights into the sources of evaporation, the transport pathways of evaporative parcels, and their residence time in the atmosphere during extreme rainfall forecasting.

Supplementary Information The online version contains supplementary material available at https://doi.org/10.1007/s00382-025-07712-w.



Acknowledgements The present study is funded through the project TRACing moisture sources of extreme rainfall over India-a tool for Better monsoon pRedIction at Synoptic TImescales (TRAC-BRISTI), which was in turn supported by a 2023/24 Global Partnership Award from the University of Southampton. DD recognise the efforts of the University of Southampton and National Oceanography Centre Southampton officials for their help in organising a symposium (comprising the co-authors) over 23-24 November 2023 at the National Oceanography Centre in Southampton (UK). This work used JASMIN, the UK collaborative data analysis facility. DD would like to acknowledge Dr. Jeffrey Blundell from the University of Southampton, UK for his support in setting up TRACMASS on JASMIN. LJ would like to thank the support from the Natural Environmental Research Council [grant number NE/S007210/1]. AT is supported by the National Centre for Atmospheric Science through the NERC National Capability International Programme Award (NE/X006263/1). AC gratefully acknowledges the financial support given by the Indian Institute of Tropical Meteorology, Ministry of Earth Sciences, Government of India (Ref. No. 11TM/MM-111/2024/A1-P06/SO-006) to conduct research under Monsoon Mission-III.

Author Contributions All authors contributed to the study conception and design. Material preparation, data collection and analysis were performed by DD, LJ and AR. The manuscript is written by DD with inputs from all the coauthors. All authors read and approved the manuscript.

Funding The present study is funded through the project TRACing moisture sources of extreme rainfall over India-a tool for Better monsoon pRedIction at Synoptic TImescales (TRAC-BRISTI), which was in turn supported by a 2023/24 Global Partnership Award from the University of Southampton.

Declarations

Conflict of interest The authors declare no Conflict of interest

Ethics approval and consent to participate Not applicable

Data availability ERA5 hourly data on single levels has been accessed through Copernicus Climate Change Service (2023): ERA5 hourly data on single levels from 1940 to present. Copernicus Climate Change Service (C3S) Climate Data Store (CDS), https://doi.org/10.24381/ cds.adbb2d47 (Accessed on 21-SEP-2023). ERA5 model level analysis data is taken from European Centre for Medium-Range Weather Forecasts (2021): ECMWF ERA5: model level analysis parameter data. Centre for Environmental Data Analysis, 04-AUG-2024. https:// catalogue.ceda.ac.uk/uuid/f809e61a61ee4eb9a64d4957c3e5bfac. The trajectory files used to generate the figures in the present study are now put in an open source website at https://doi.org/10.5281/zenodo. 12696903

Materials availability Not applicable

Code availability The Lagrangian tracing model TRACMASS is open access and can be download through https://doi.org/10.5281/zenodo. 4337926 and also using the open source repository in https://github. com/TRACMASS/tracmass

Open Access This article is licensed under a Creative Commons Attribution 4.0 International License, which permits use, sharing, adaptation, distribution and reproduction in any medium or format, as long as you give appropriate credit to the original author(s) and the source, provide a link to the Creative Commons licence, and indicate if changes were made. The images or other third party material in this article are

included in the article's Creative Commons licence, unless indicated otherwise in a credit line to the material. If material is not included in the article's Creative Commons licence and your intended use is not permitted by statutory regulation or exceeds the permitted use, you will need to obtain permission directly from the copyright holder. To view a copy of this licence, visit http://creativecommons.org/licenses/by/4.0/.

References

- Adler C, Wester P, Bhatt I, Huggel C, Insarov G, Morecroft M, Muccione V, Prakash A (2022) Cross-Chapter Paper 5: Mountains. In: Climate Change 2022: Impacts, Adaptation and Vulnerability. Contribution of Working Group II to the Sixth Assessment Report of the Intergovernmental Panel on Climate Change. Cambridge University Press, Cambridge, pp. 2273-2318
- Aldama-Campino A, Döös K, Kjellsson J, Jönsson B (2020) December. Tracmass: Formal release of version 7.0
- Baidya SK, Shrestha ML, Sheikh MM (2008) Trends in daily climatic extremes of temperature and precipitation in nepal. J Hydrol Meteorol 5(1):38-51
- Baudouin JP, Herzog M, Petrie CA (2020) Cross-validating precipitation datasets in the indus river basin. Hydrol Earth Syst Sci 24(1):427-450
- Berglund S, Döös K, Campino AA, Nycander J (2021) The water mass transformation in the upper limb of the overturning circulation in the southern hemisphere. J Geophys Res: Oceans 126(8): e2021JC017330
- Berglund S, Döös K, Groeskamp S, McDougall TJ (2022) The downward spiralling nature of the north atlantic subtropical gyre. Nat Commun 13(1):2000
- Dash P, Punia M (2019) Governance and disaster: analysis of land use policy with reference to uttarakhand flood 2013, india. Int J Disaster Risk Reduc 36:101090
- Dey D, Döös K (2019) The coupled ocean-atmosphere hydrologic cycle. Tellus A 71(1):1650413
- Dey D, Döös K (2020) Atmospheric freshwater transport from the atlantic to the pacific ocean: A lagrangian analysis. Geophys Res Lett 47(6): e2019. https://doi.org/10.1029/2019GL086176. https:// agupubs.onlinelibrary.wiley.com/doi/pdf/10.1029/2019GL086176
- Dimri A, Thayyen R, Kibler K, Stanton A, Jain S, Tullos D, Singh V (2016) A review of atmospheric and land surface processes with emphasis on flood generation in the southern himalayan rivers. Sci Total Environ 556:98-115
- Döös K (1995) Interocean exchange of water masses. J Geophys Res Oceans 100(C7):13499-13514
- Döös K, Jönsson B, Kjellsson J (2017) Evaluation of oceanic and atmospheric trajectory schemes in the tracmass trajectory model v6.0. Geosci Model Dev 10(4):1733-1749
- Döös K, Nycander J, Coward AC (2008) Lagrangian decomposition of the deacon cell. J Geophys Res Oceans 113:7
- Dou J, Wu Z, Zhou Y (2017) Potential impact of the may southern hemisphere annular mode on the indian summer monsoon rainfall. Clim Dvn 49:1257-1269
- Francis JA, Vavrus SJ (2015) Evidence for a wavier jet stream in response to rapid arctic warming. Environ Res Lett 10(1):014005
- Geen R, Thomson SI, Screen JA, Blackport R, Lewis NT, Mudhar R, Seviour WJ, Vallis GK (2023) An explanation for the metric dependence of the midlatitude jet-waviness change in response to polar warming. Geophys Res Lett 50(21):e202
- Gogoi C, Goswami DC, Phukan S (2013) Flood risk zone mapping of the subansiri sub-basin in assam, india. Int J Geomat Geosci 4(1):75-88



- Gupta A, Konduru RT, Singh V (2023) Satellite sensed summer monsoon torrential rain events characteristics along the himalayan regions of north india and their dynamics. Atmos Res 296:107077
- Gupta V, Syed B, Pathania A, Raaj S, Nanda A, Awasthi S, Shukla DP (2024) Hydrometeorological analysis of july-2023 floods in himachal pradesh, india. Nat Hazards 8:1–26
- Hersbach H, Bell B, Berrisford P, Hirahara S, Horányi A, Muñoz-Sabater J, Nicolas J, Peubey C, Radu R, Schepers D, Simmons A, Soci C, Abdalla S, Abellan X, Balsamo G, Bechtold P, Biavati G, Bidlot J, Bonavita M, De Chiara G, Dahlgren P, Dee D, Diamantakis M, Dragani R, Flemming J, Forbes R, Fuentes M, Geer A, Haimberger L, Healy S, Hogan RJ, Hólm E, Janisková M, Keeley S, Laloyaux P, Lopez P, Lupu C, Radnoti G, de Rosnay P, Rozum I, Vamborg F, Villaume S, Thépaut JN (2020) The era5 global reanalysis. Q J R Meteorol Soc 146(730):1999–2049. https://doi.org/10.1002/qj.3803. (https://rmets.onlinelibrary.wiley.com/doi/pdf/10.1002/qj.3803)
- Houze R, McMurdie L, Rasmussen K, Kumar A, Chaplin M (2017) Multiscale aspects of the storm producing the June 2013 flooding in uttarakhand, india. Mon Weather Rev 145(11):4447–4466
- Huffman GJ, Bolvin DT, Braithwaite D, Hsu KL, Joyce RJ, Kidd C, Nelkin EJ, Sorooshian S, Stocker EF, Tan J, Wolff DB, Xie P (2020) Integrated multi-satellite retrievals for the global precipitation measurement (GPM) mission (IMERG). Springer International Publishing, Cham, pp 343–353
- Hunt KM, Turner AG, Schiemann RK (2021) How interactions between tropical depressions and western disturbances affect heavy precipitation in south asia. Mon Weather Rev 149(6):1801–1825
- Hunt KM, Turner AG, Shaffrey LC (2018) Extreme daily rainfall in pakistan and north india: Scale interactions, mechanisms, and precursors. Mon Weather Rev 146(4):1005–1022
- Hunt KMR, Turner AG, Shaffrey LC (2018) The evolution, seasonality and impacts of western disturbances. Q J R Meteorol Soc 144(710):278–290. https://doi.org/10.1002/qj.3200
- Jenamani RK, Dash S (2005) A study on the role of synoptic and semipermanent features of indian summer monsoon on it's rainfall variations during different phases of el-nino. Mausam 56(4):825–840
- Joseph S, Sahai AK, Sharmila S, Abhilash S, Borah N, Chattopadhyay R, Pillai PA, Rajeevan M, Kumar A (2015) North indian heavy rainfall event during June 2013: diagnostics and extended range prediction. Clim Dyn 44:2049–2065
- Joshi V, Kumar K (2006) Extreme rainfall events and associated natural hazards in alaknanda valley, indian himalayan region. J Mt Sci 3:228–236
- Kaur S, Gupta P (2017) Devastating rainstorm of June-2013 in uttarakhand. Mausam 68(4):633–642
- Kjellsson J, Döös K (2012) Lagrangian decomposition of the hadley and ferrel cells. Geophys Res Lett 39:15
- Lindell MK, Arlikatti S, Huang SK (2019) Immediate behavioral response to the june 17, 2013 flash floods in Uttarakhand, North India. Int J Disaster Risk Reduc 34:129–146
- Nagamani K, Mishra AK, Meer MS, Das J (2024) Understanding flash flooding in the himalayan region: a case study. Sci Rep 14(1):7060
- Nandargi S, Dhar O (2012) Extreme rainstorm events over the northwest himalayas during 1875–2010. J Hydrometeorol 13(4):1383–1388
- Peixoto JP, Oort AH (1992) Physics of climate
- Raghuvanshi AS, Agarwal A (2024) Multiscale dynamics of transient merging between western disturbances and monsoonal lows: Connections to the July 2023 flood in himachal pradesh. Atmos Res 304:107401
- Rana N, Singh S, Sundriyal Y, Juyal N (2013) Recent and past floods in the alaknanda valley: causes and consequences. Curr Sci 105(9):1209–1212

- Ranalkar MR, Chaudhari HS, Hazra A, Sawaisarje G, Pokhrel S (2016) Dynamical features of incessant heavy rainfall event of June 2013 over uttarakhand, india. Nat Hazards 80:1579–1601
- Rawat N, Thapliyal A, Purohit S, Negi GS, Dangwal S, Rawat S, Aswal A, Kimothi M (2016) Vegetation loss and ecosystem disturbances on kedargad mandakini subwatershed in rudraprayag district of uttarakhand due to torrential rainfall during June 2013. Int J Adv Remote Sens GIS 5(4):1662–1669
- Ray K, Bhan S, Sunitha Devi S (2014) A meteorological analysis of very heavy rainfall event over uttarakhand during 14–17 june, 2013. India Meteorological Department, Delhi, pp 37–54
- Revadekar J, Varikoden H, Preethi B, Mujumdar M (2016) Precipitation extremes during indian summer monsoon: role of cyclonic disturbances. Nat Hazards 81:1611–1625
- Singh O, Kumar M (2013) Flood events, fatalities and damages in india from 1978 to 2006. Nat Hazards 69:1815–1834
- Stäubli, A., Nussbaumer SU, Allen SK, Huggel C, Arguello M, Costa F, Hergarten C, Martínez R, Soto J, Vargas R, et al (2018) Analysis of weather-and climate-related disasters in mountain regions using different disaster databases. Climate change, extreme Events and disaster risk reduction: towards sustainable development goals 17–41
- Tamarin-Brodsky T, Harnik N (2024) The relation between rossby wave-breaking events and low-level weather systems. Wea Clim Dyn 5(1):87–108
- Toptunova O, Motsakov M, Koval A, Ermakova T, Didenko K (2025) Impact of sudden stratospheric warming on tropospheric circulation and a cold wave formation: the case of the january 2019 event. Atmos Res 107:998
- Van Sebille E, Griffies SM, Abernathey R, Adams TP, Berloff P, Biastoch A, Blanke B, Chassignet EP, Cheng Y, Cotter CJ et al (2018) Lagrangian ocean analysis: fundamentals and practices. Ocean Model 121:49–75
- Vellore RK, Bisht JS, Krishnan R, Uppara U, Di Capua G, Coumou D (2020) Sub-synoptic circulation variability in the himalayan extreme precipitation event during June 2013. Meteorol Atmos Phys 132:631–665
- Vellore RK, Kaplan ML, Krishnan R, Lewis JM, Sabade S, Deshpande N, Singh BB, Madhura R, Rama Rao M (2016) Monsoon-extratropical circulation interactions in himalayan extreme rainfall. Clim Dyn 46:3517–3546
- Vellore RK, Krishnan R, Pendharkar J, Choudhury AD, Sabin T (2014) On the anomalous precipitation enhancement over the himalayan foothills during monsoon breaks. Clim Dyn 43:2009–2031
- Vogel MM, Hauser M, Seneviratne SI (2020) Projected changes in hot, dry and wet extreme events' clusters in cmip6 multi-model ensemble. Environ Res Lett 15(9):094021
- Webster PJ, Magana VO, Palmer T, Shukla J, Tomas R, Yanai M, Yasunari T (1998) Monsoons: processes, predictability, and the prospects for prediction. J Geophys Res Oceans 103(C7):14451–14510
- Zha P, Wu Z (2025) Can the tibetan plateau freeze-thaw state influence the interannual variations of the east asian summer monsoon during meiyu season? Clim Dyn 63(1):72
- Zhang P, Wang B, Wu Z, Jin R, Cao C (2024) Intensified gradient la niña and extra-tropical thermal patterns drive the 2022 east and south Asian seesaw extremes. NPJ Clim Atmos Sci 7(1):47
- **Publisher's Note** Springer Nature remains neutral with regard to jurisdictional claims in published maps and institutional affiliations.



Authors and Affiliations

Dipanjan Dey^{1,2} · Ligin Joseph² · Arkaprava Ray¹ · Robert Marsh² · Nikolaos Skliris² · Andrew G. Turner^{3,4} · D. C. Ayantika⁵ · Parthasarathi Mukhopadhyay⁶ · Arun Chakraborty⁷ · Sourav Sil¹

 □ Dipanjan Dey dipanjandey@iitbbs.ac.in; d.dey@soton.ac.uk

Ligin Joseph lj3n23@soton.ac.uk

Arkaprava Ray ar31@iitbbs.ac.in

Robert Marsh r.marsh@soton.ac.uk

Nikolaos Skliris n.skliris@soton.ac.uk

Andrew G. Turner a.g.turner@reading.ac.uk

D. C. Ayantika ayantika@tropmet.res.in

Parthasarathi Mukhopadhyay parthasarathym@iiserbpr.ac.in

Arun Chakraborty arunc@coral.iitkgp.ac.in

Sourav Sil souravsil@iitbbs.ac.in

- School of Earth, Ocean and Climate Sciences, Indian Institute of Technology Bhubaneswar, Jatni, Khordha, Odisha 752050, India
- School of Ocean and Earth Science, University of Southampton, Southampton SO14 3ZH, UK
- Department of Meteorology, University of Reading, Reading RG6 6ET, UK
- National Centre for Atmospheric Science, University of Reading, Reading RG6 6BB, UK
- Centre for Climate Change Research, Indian Institute of Tropical Meteorology, Dr. Homi Bhabha Road, Pune, Maharashtra 411 008, India
- Department of Earth and Environmental Sciences, Indian Institute of Science Education and Research, Berhampur, Odisha 760003, India
- Centre for Ocean, River, Atmosphere and Land Sciences, Indian Institute of Technology Kharagpur, Kharagpur, West Bengal 721302, India

